SOFT X-RAY OBSERVATION OF A LARGE-SCALE CORONAL WAVE AND ITS EXCITER

HUGH S. HUDSON[1,*], JOSEF I. KHAN[2,**], JAMES R. LEMEN[3],
NARIAKI V. NITTA[3] and YUTAKA UCHIDA[4,†]

[1]*Solar Physics Research Corp., U.S.A. (e-mail: hhudson@spd.aas.org)*
[2]*Mullard Space Science Laboratory, University College London, Holmbury Saint Mary, Dorking, Surrey, RH5 6NT, U.K.*
[3]*Lockheed Martin Palo Alto Research Laboratory, U.S.A.*
[4]*Science University of Tokyo, Japan*

Abstract. Recent extreme ultraviolet (EUV) observations from SOHO have shown the common occurrence of flare-associated global coronal waves strongly correlated with metric type II bursts, and in some cases with chromospheric Moreton waves. Until now, however, few direct soft X-ray detections of related global coronal waves have been reported. We have studied *Yohkoh* Soft X-ray Telescope (SXT) imaging observations to understand this apparent discrepancy, and describe the problems in this paper. We have found good X-ray evidence for a large-scale coronal wave associated with a major flare on 6 May 1998. The earliest direct trace of the wave motion on 6 May consisted of an expanding volume within 20 Mm (projected) of the flare-core loops, as established by loop motions and a dimming signature. Wavefront analyses of the soft X-ray observations point to this region as the source of the wave, which began at the time of an early hard X-ray spike in the impulsive phase of the flare. The emission can be seen out to a large radial distance (some 220 Mm from the flare core) by SXT, and a similar structure at a still greater distance by EIT (the Extreme Ultraviolet Imaging Telescope) on SOHO. The radio dynamic spectra confirm that an associated disturbance started at a relatively high density, consistent with the X-ray observations, prior to the metric type II burst emission onset. The wavefront tilted away from the vertical as expected from refraction if the Alfvén speed increases with height in the corona. From the X-ray observations we estimate that the electron temperature in the wave, at a distance of 120 Mm from the flare core, was on the order of 2 –4 MK, consistent with a Mach number in the range 1.1–1.3.

1. Introduction

Two lines of evidence showed many years ago that large-scale shock waves can accompany a solar flare: the meter-wave type II burst (e.g., Wild, Smerd, and Weiss, 1963) and the 'Moreton wave' (Moreton, 1960; Moreton and Ramsey, 1960; Moreton, 1961). The evidence for the latter consists of a rapidly-expanding front

*Present address: Space Sciences Laboratory, University of California Berkeley CA 94720-7450, U.S.A.
**Present address: Tuorla Observatory, University of Turku, Väisäläntie 20, FIN-21500 Piikkiö, Finland
†deceased.

resulting in Hα signatures; the high speeds (800–2500 km s^{-1}) and general morphology strongly suggested an identification of the chromospheric signatures with the skirt of a globally expanding coronal wave, roughly hemispherical, concentric on a point near the flare site, and starting at what we now term the 'impulsive phase' of the flare. Uchida (1968, 1974) described both sets of phenomena as manifestations of a weak fast-mode MHD shock wave. This theory explained the refraction of a wave around a solar active region as the result of the spatial variation of the Alfvén speed in the corona, as modeled in the eikonal approximation.

Neither the radio spectra nor the Hα imaging observations show the coronal waves directly. The Hα data often show sectors of a wavefront in the chromosphere, emanating roughly concentrically from the flaring region. They also show the 'winking filament' phenomenon, explained (e.g., Ramsey and Smith, 1966) as Doppler shifts when the filament material bobs up and down in response to the large-scale wave in the corona. The type II burst appears at meter wavelengths and exhibits a slow drift to longer wavelengths; the electromagnetic radiation originates in Langmuir turbulence excited by the shock front (e.g., Nelson and Melrose, 1985). The resulting emission is at the plasma frequency and its harmonics, allowing a good estimate of the plasma density at the point of emission. A meter-wave imager such as the Nançay radioheliograph (Kerdraon and Delouis, 1997) can map this emission, but the event discussed in this paper occurred outside the Nançay observing window and only dynamic spectra are available.

In principle soft X-ray or EUV observations of high-temperature coronal emissions should show us such a flare-associated wave more directly, as a result of density and temperature variations as the wave passes through the medium and compresses it. Observations from EIT (e.g., Thompson *et al.*, 1998; 2000a) and TRACE (the Transition Region and Chromospheric Explorer; Wills-Davey and Thompson, 1999) have in fact demonstrated that large-scale wave disturbances do frequently occur, in close association with flares. Unfortunately, few analogous observations have been reported from the *Yohkoh* Soft X-ray Telescope (SXT) data; this is a puzzle because the density and temperature modulations due to such a wave should cause detectable emissivity increases, if in fact the ambient corona can be detected in the first place. Khan and Aurass (2002) report one clear example, which successfully identifies soft X-ray, EUV, Hα, and meter-wave observations for an event of 3 November 1997. This event occurred outside the *Yohkoh* flare mode and thus had poor data sampling. Such clear examples as that event and the event discussed in this paper (see Hudson and Karlický, 2000, for a preliminary report) remain rare, in spite of efforts to optimize the SXT observations for such events. Recently, Narukage *et al.* (2002) report another event observed in soft X-rays and Hα.

In this paper we describe and interpret the mechanics of soft X-ray detection, in order to understand why wave observations have not occurred more commonly in the SXT data. This material has been put in Appendix A, a list of the factors
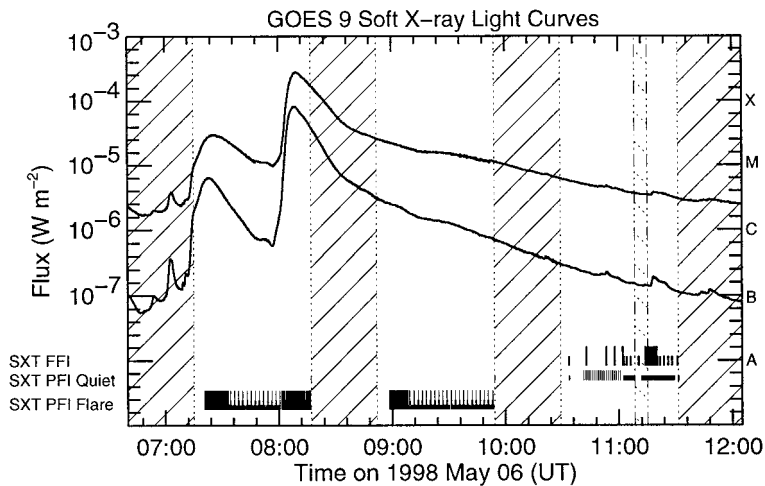
Figure 1. Soft X-ray time history (GOES data, upper curve 1–8 Å) for the flare of 6 May 1998, indicating the times of the *Yohkoh* observations. *Diagonal shading* shows times of *Yohkoh* orbit night and particle contamination, and *tick marks at the bottom* show times of SXT images (*dense shading* shows high telemetry rate.) Figure 2 shows details at the time of the wave observations.

involved in the detectability of waves, and in Appendix B, which provides an analysis of the SXT spectral response to a wave.

The observations reported below add to our knowledge of the physical nature of the source of a metric type II burst, which we believe we have now detected at high resolution within 20 Mm (0.03 $R_\odot$) of the flare core. The 6 May event is probably the best yet found with which soft X-ray observations can be used to study the origin of such a disturbance. The wave itself can be observed to the edge of the SXT field of view, a distance of some 220 Mm (0.3 $R_\odot$) from the flare core. Other observations of metric type II bursts and soft X-ray ejecta have been reported by Gopalswamy *et al.* (1997), Klassen *et al.* (1999), Klein *et al.* (1999), and Pohjolainen *et al.* (2001). With these soft X-ray observations we have begun to look with high angular resolution at the dynamics of hot material near the innermost core of the flare. We believe that we have localized the beginning of the wave disturbance to an expansion originating at a localized source appearing at the start of the impulsive phase, temporally associated with an initial hard X-ray spike but located at some distance from the bright core loops of the flare.

Section 2 gives the observational background for this study and Section 3 describes the *Yohkoh* observations. We discuss physical conditions in the flare and wave in Section 4. The CD-ROM enclosure for this paper consists of movie sequences, which clarify many of the points discussed in the paper.

2. Observational Background

High-resolution observations of the corona from *Yohkoh*, SOHO, and TRACE add to our understanding the behavior of large-scale waves in the corona. Heretofore these have been known mainly indirectly in the form of type II radio bursts and chromospheric Moreton waves, although some events have been imaged by radio-heliographs (e.g., Kai, 1969; Harvey, Martin, and Riddle, 1974). The X-ray and EUV observations can show *direct* emission from the waves themselves. Although the *Yohkoh* soft X-ray observations did not reveal such waves just after launch (1991), the SOHO EIT data soon did (Moses *et al.*, 1997; Thompson *et al.*, 1998, 1999).

The *Yohkoh* data did reveal the common existence of eruptions visible in soft X-rays (Klimchuk *et al.*, 1994), as first seen in the *Skylab* observations (Rust and Hildner, 1978). Much research has followed this beginning, and the X-ray data show many spectacular examples of expanding structures clearly identifiable with magnetic loops filled with hot, dense gas (Hudson *et al.*, 1996; Gopalswamy *et al.*, 1998) and associated with coronal mass ejections (Nitta and Akiyama, 1999; Khan and Hudson, 2000), as well as diffuse 'dimmings' resulting from coronal depletions (e.g., Hudson and Webb, 1997) of several types. The novelty of the new X-ray and EUV data is their ability to detail coronal dynamics against the disk, as well as above the limb.

The relationship between flare (or non-flare) ejecta and global waves has remained problematic. The meter-wave type II bursts, long known to have a close flare correlation, have been identified as blast waves visible as weak MHD fast-mode shocks (Uchida, 1968). These could arise from a 'pressure pulse' resulting from the flare energization. Here we take the term 'pressure pulse' literally to mean a limited transient expansion resulting from a sudden increase of pressure in a localized disturbance not causing a lasting displacement of the medium. On the other hand the longer-wavelength interplanetary type II bursts, physically related to ejecta associated with coronal mass ejections (CMEs) by *in situ* observations, instead appear to be 'driven waves' in which the moving medium continues to energize the wave. The close relationship between flares and CMEs has delayed the understanding of the physical origin of these waves. Occam's Razor encourages the idea that the coronal and interplanetary waves are the same phenomenon (e.g., Cliver, Webb, and Howard, 1999). However recent higher-resolution observations have sharpened the distinction between the two kinds of global wave, while at the same time identifying the metric type II burst in detail with flare ejecta (Gopalswamy *et al.*, 1997; Klein *et al.*, 1999). The question remains the same in either case – what induces the flare ejecta, whether contained or not?

The event discussed in this paper has already been presented by Khan and Hudson (2000) and by Hudson and Karlický (2000) and was among the events selected for intensive study at a Coordinated Data Analysis Workshop (see the papers in *J. Geophys. Res.* **106**). The NOAA active region 8210 produced two X-
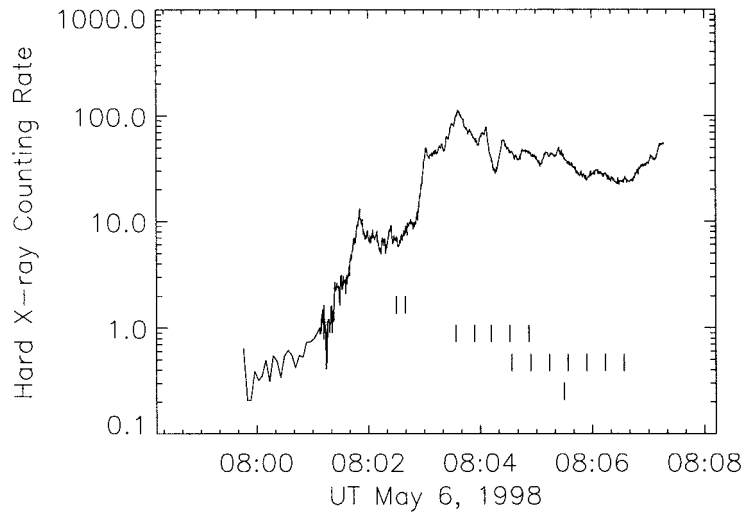
Figure 2. Timing of SXT images in comparison with the hard X-ray data (*Yohkoh* HXT M2 channel, 33–53 keV band). The *tick marks* show the times of clear wave detection (in the AlMg filter only). *Upper row*: full resolution (2.5′ field of view); *second row*: half resolution (5′ field of view); *third row*: quarter resolution (10′ field of view); *fourth row*: the type II onset time (Potsdam).

class flares and also displayed the interesting morphology of CME association with transequatorial interconnecting loop systems described by Khan and Hudson (see also Delannèe and Aulanier, 1999; Thompson *et al.*, 2000b; Pohjolainen *et al.*, 2001; Wang *et al.*, 2002). We only investigate the 6 May X2.7 flare in detail here, but Khan and Hudson note that events on 8 May and 9 May were approximately homologous. At the time of occurrence of the 6 May 1998 event, the active region was at approximately S17 W64. Table I summarizes the analysis of the May 6 event, with the table entries to be explained in later sections as they are discussed. Note that the location of the event near the limb will allow us to study the vertical structure of the disturbance as it evolves.

3. Observations of the 6 May 1998 Event

3.1. IMAGING

Figure 1 shows the time development of the 6 May flare with GOES soft X-ray fluxes as a reference, indicating the times of the *Yohkoh* SXT observations; these are also shown at higher time resolution relative to the hard X-ray light curve in Figure 2. Table I gives specific reference times and more details about the flare properties. *Yohkoh* had already entered flare mode (restricted field of view and high cadence) as a result of an earlier flare in the same active region. A good pattern of telemetry contacts allowed flare mode to continue longer than usual.

H. S. HUDSON ET AL.

TABLE I
Properties of the X-class flare of 6 May 1998.

GOES X-ray times	07:58/08:09/08:20 UT[a]
Flare position	S15 W70
Classifications	X2.7; 1N; metric type II, III, IV
Active region	NOAA 8210
Character	Impulsive/LDE
Wave radiant time (5″ pixels)	08:01:05 UT
Yohkoh high-rate data start	08:01:14 UT
Initial hard X-ray peak	08:01:51 UT (HXT 33–53 keV)
Wave radiant time (10″ pixels)	08:02:00 UT
Dimming reference time	08:02–08:03 UT
Soft X-ray wave signatures	08:02:35–08:06:34 UT
Type II onset	08:03:20 UT
Major hard X-ray peak	08:03:37 UT (HXT 33–53 keV)
North footpoint (flare core) flash	08:03:30 UT
Time of half maximum loop pressure	08:03:50 UT
Parameter reference time (core loop)	08:07:58 UT
Flux (Be filter)	1.3×10^7 DN s^{-1}
Core loop dimension	10 Mm
Core loop density	2.9×10^{11} cm^{-3}
Core loop temperature	14 MK
Core loop pressure	1.1×10^3 dyne cm^{-2}
EIT observation time	08:10.0 UT

[a]GOES time definitions, which underestimate event duration by defining the end time as the 50% peak time.

Figure 2 shows the timing of the relevant images in the context of the hard X-ray flux observed by *Yohkoh* HXT, indicating the times of the soft X-ray images that have clearly indentifiable wave effects. The wave can be seen progressively starting from the smallest field of view to the largest. From this crude comparison of space and time we find that the earliest hard X-ray spike, or the event onset in general, corresponds better with the wave origin than does the principal hard X-ray peak. The onset time of the type II burst occurs near the midpoint of the quarter-resolution images, when the wave is approximately 2.5′ or $\sim$ 30 Mm from the flare core. SXT has therefore probably observed the wave both *before* and *after* its shock turn-on.

The SXT observations show rapidly-moving arc-shaped brightenings, not quite concentric on the flare core and most clearly visible to the north. Related features are visible in the 'full', 'half', or 'quarter' resolution images (2.45″, 4.91″, and 9.82″ pixels), respectively, at different times. We show these data in Figures 3–
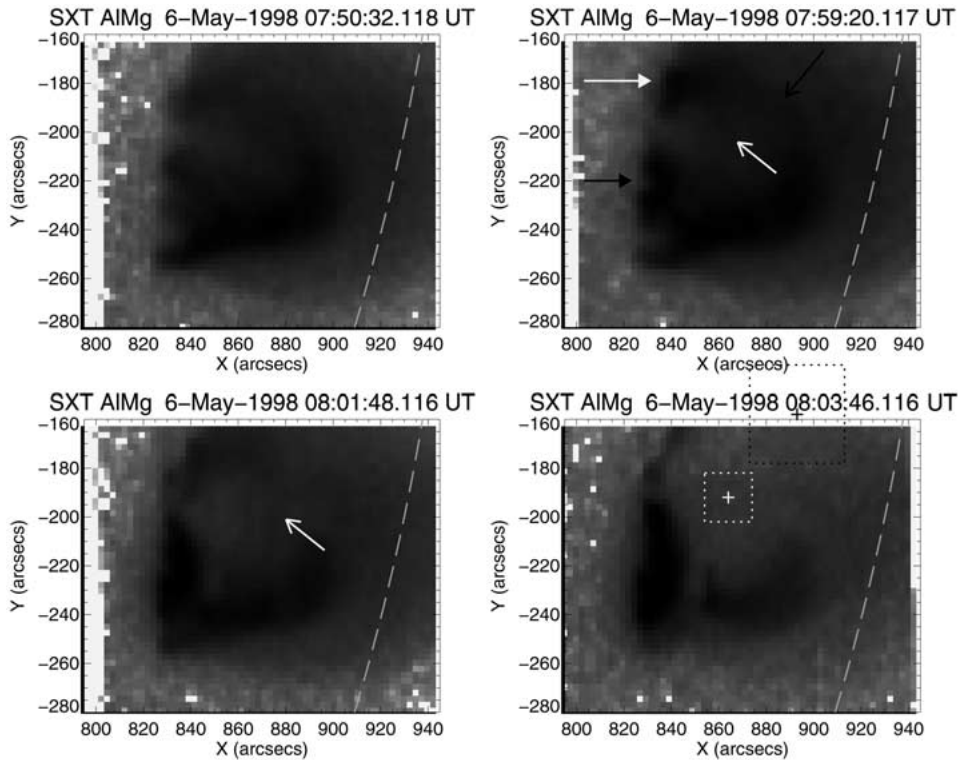
Figure 3. Soft X-ray images (AlMg filter, full resolution; N up, W to the right, as with all images in this paper) of the early development of the source region for the wave. *Arrows* on the left in the 07:59:20 UT image point to compact loop-like features, the southern (*black arrow*) one later developing into the flare-core loops. Note the dimming region to the NW of the core loops in the final frame. The white arrows in the centers of the frames at 07:59:20 UT and 08:01:48 UT show a faint feature that moves outwards across the dimming region prior to its evacuation. The *diagonal black arrow* at upper right points to the feature that disappeared during the dimming, as described in the text. The *dotted boxes* show the radiant points inferrred from the wavefront analysis described later in the text; white, $5''$ pixels, black, $10''$ pixels. For better visibility of the early faint feature, please see the CD-ROM material.

5. We interpret these moving features as direct heating via wave passage, not as the physical motion of magnetic loops. Section 5.2 presents the arguments for and against this interpretation as a wave, which on the basis of the SXT images alone is not entirely unambiguous.

The full-resolution images, at approximately 2 s sampling starting at 08:01:14 UT, give us an unprecedented view of the early development of the flare and wave (Figure 3). Prior to these high-rate data we can already see a feature (diagonal white arrows) moving slowly outwards in the vicinity of the wave source region (to be discussed in detail later) as well as a bright, compact loop that eventually extends to become the flare core loop structure. The horizontal white arrow points to a loop-like feature at the footpoint of the dimming feature to the north

of the flare core. The soft X-ray images of the core loops do not show prominent footpoint brightening. The last panel of Figure 3 shows the dimming to the NW of the core loops caused by the outward motions of the structures (diagonal black arrow in the panel at the upper right) seen in the earlier frames, to be discussed later.

The SXT images sequences at half and quarter resolution show the outward motion of the wave best. We display these as running differences in the multiple-panel Figures 4 and 5, respectively. The running-difference technique nicely suppresses the slower variations due to the bright flare loops (except for the saturation artifacts), but one must bear in mind that one image of the wave in a differenced pair may overlap the related feature on the other image, resulting in a distortion because of the image confusion; successive SXT images for these differences are only about 20 s apart, corresponding to only about 3.5 pixels of motion at 600 km s^{-1}.

From the SXT observations we estimate the projected footpoint separation of the flare core loops (black arrow in the 07:59:20 UT panel of Figure 3) to be about 6 pixels, or approximately 10 Mm; the simultaneous hard X-ray images from the *Yohkoh* HXT imager confirm that the initial hard X-ray spike came from this structure and do show the expected hard X-ray footpoint brightening (Figure 6). The loop orientation, concave to the east, roughly matches the appearance expected of a loop lying in a vertical plane. We refer to this compact loop as the flare core, and take its geometric center as a position reference. Figure 6 shows the soft and hard X-ray morphology at the time of the initial hard X-ray spike (08:01:51 UT).

On larger scales we can see the structure of the active-region loops. The large loop structure to the north of the flare core appeared to explode outward, especially to the north and northwest, and Figure 7 characterizes the timing of this motion via a sudden dimming signature. Sudden dimming implies rapid expansion and/or ejection, which we can see directly in the images but not well enough to measure velocities. The initial location of the northern leg of the expanding large loop structure was at a projected distance of about 16 Mm along the line at position angle 330° from the flare core. We estimate the half-intensity time of the dimming signature (Figure 7) to be at about $\sim 08{:}02$ UT to $\sim 08{:}03$ UT, depending upon location within the region. For comparison, the peak of the initial hard X-ray burst occurred at 08:01:51 UT, consistent with the estimated radiant times (see Table I for the chronology). The pressure increase in the flare core loop reached half-maximum at about 08:03:50 UT (see Section 4), with an estimated error of about ten seconds. The start of the brightening of the type II emission followed all of these epochs by two minutes or more, but the drifting decimeter emission was more or less contemporaneous with the early signatures (see Figure 11).

To summarize the analysis of the images, the waves and motions seem to emanate from an initial development just to the north and northwest of the flare core loops. The initial rapidly moving structure had been a stable part of the active region prior to the flare. The rapid motion resembles a pivoting of this coronal structure at its footpoint; this footpoint region also dims measurably over a larger
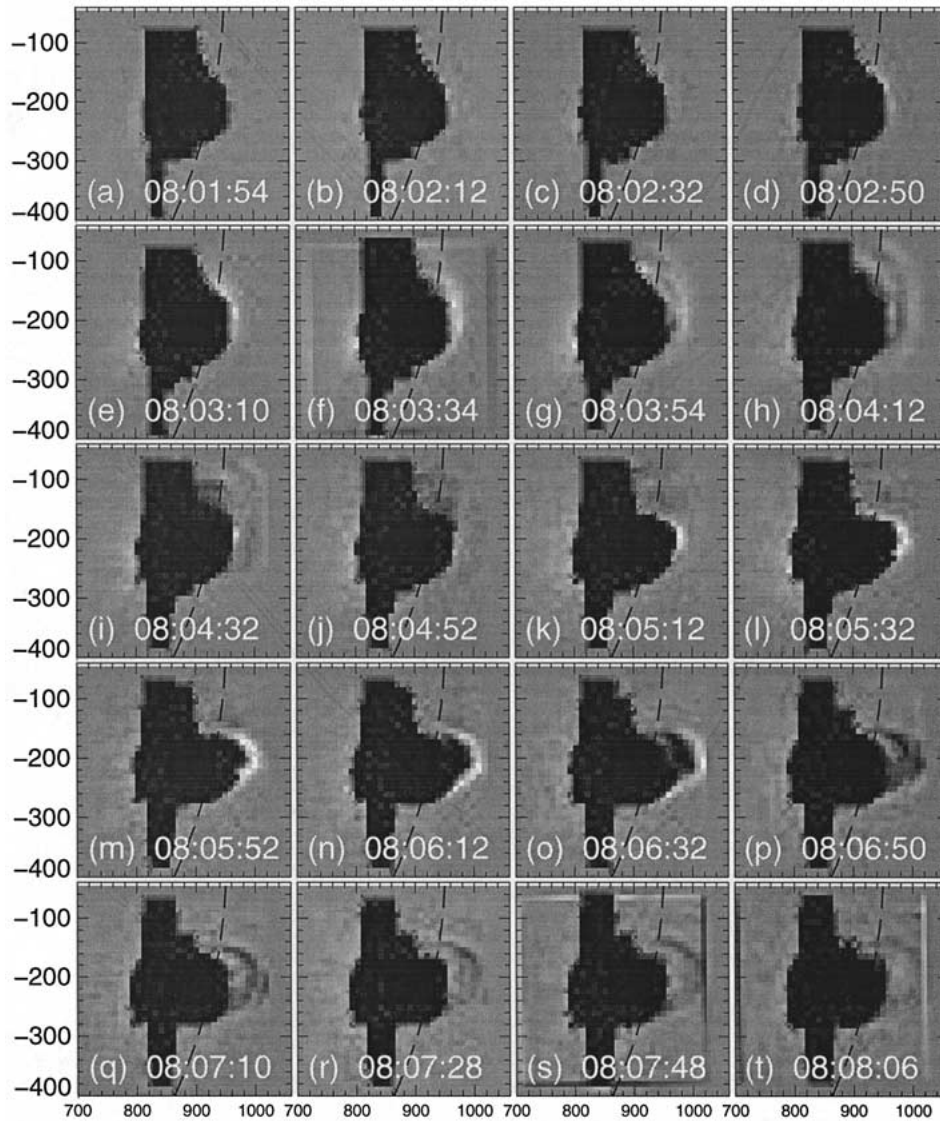
Figure 4. Running difference images taken from the AlMg half-resolution (5″ pixel size) sequence, with a first reference image at 08:01:36 UT. These images show the pattern of the early wave development to be a series of nearly concentric and circular fronts to the west of the core loops. Some frames (e.g., g, h, and i) show multiple wavefronts. Later in the event (l, m, n . . .) one can see the slower-moving flare ejecta moving more directly westward. The featureless black regions show areas of image saturation. Limb indicated by *dashed black line*.
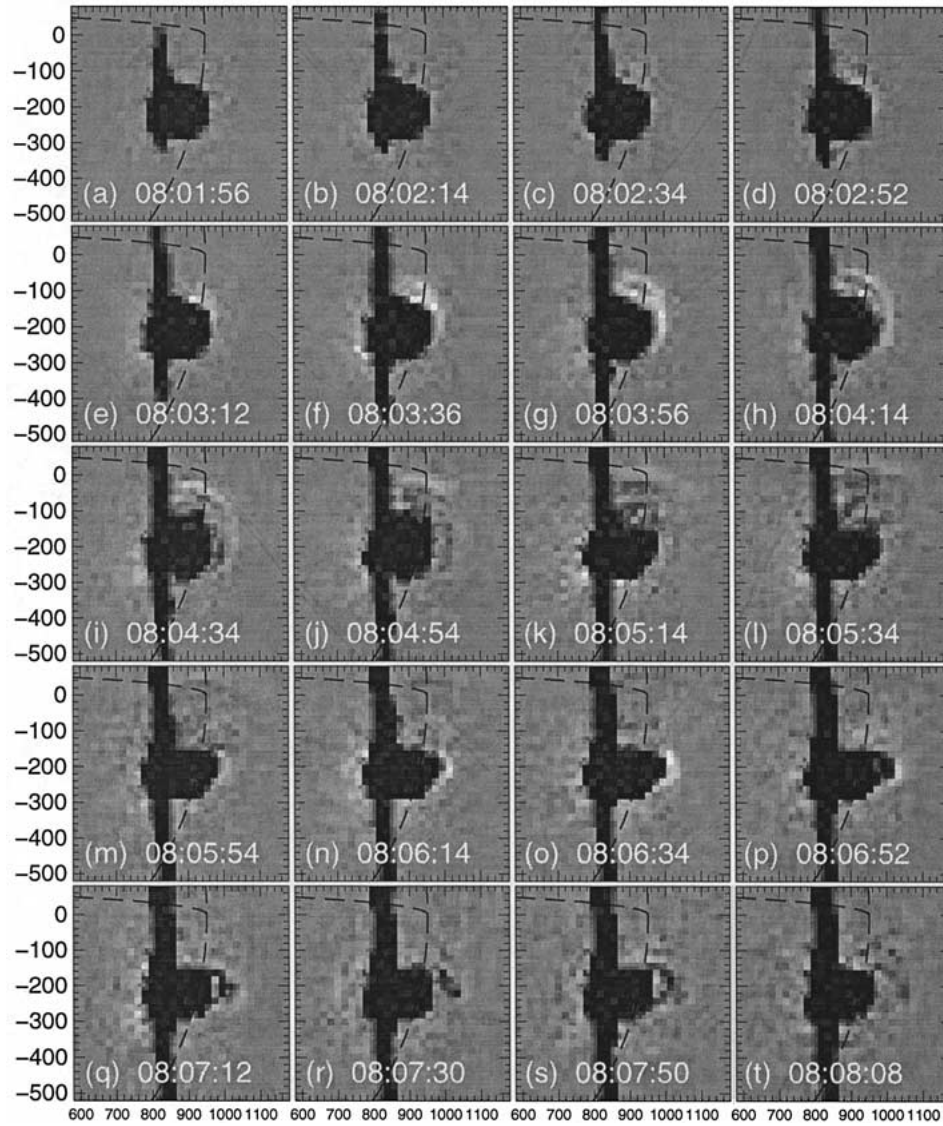
Figure 5. As for Figure 4, but showing the AlMg quarter-resolution (10″ pixel size) sequence; first reference image at 08:01:38 UT. Limb and equator are indicated by *dashed black lines*. Note the tilting of the wavefronts by comparison of h and i, for example, and the loop-like ejecta appearing in frame p.
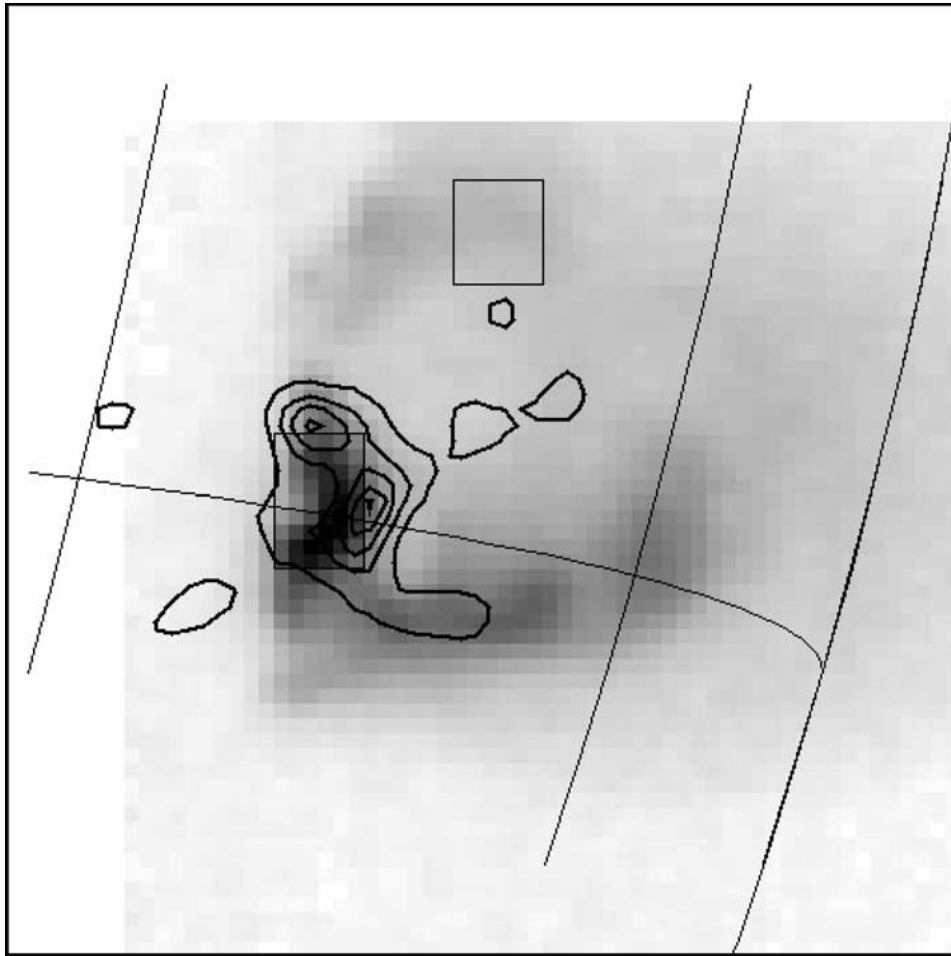
Figure 6. Soft X-ray image (Al.1 filter, full resolution, negative image) of the flare region at 08:01:52 UT; field of view 2.5′. The *grid lines* show S15 and W60, W75, W90. The feature first showing the wave effects (see text) can be seen to the north of the bright core loop structure of the flare. This compact core (scale ~ 10 Mm) is the object of the pressure-pulse analysis described in Section 4. The overlaid *thick contours* show an HXT image in the 33–53 keV band for a 20-s integration centered on the SXT image time. The *thin boxes* show two integration regions for the light curves of Figure 7: one covering the compact core loop, and one in the dimming feature.

area. We interpret the swinging motion as part of a sudden expansion of the volume south of it, but north of the flare core. The expansion was especially prominent to the north and to the west, as can be seen from Figure 3. Slower motions apparently within this region (see Figure 3 and the movies on the CD-ROM enclosure) preceded the sudden expansion.
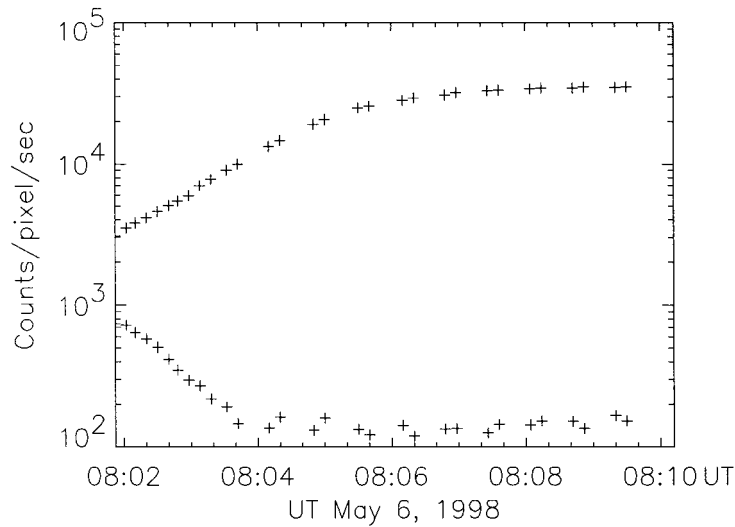
Figure 7. Light curves (average DN/s per pixel in the Be filter) for the flare core (*upper*) and the dimming region (*lower*), as marked by the boxes in Figure 6. After 08:04 UT the signal level in the dimming region shows only noise.

3.2. KINEMATICS

Some of the difference images (e.g., Figure 4(h)) suggest two ripples, but the quality of the images makes it difficult to determine much about the structure. Other images showing the X-ray wave at quarter resolution (times marked on Figure 2 and shown as running differences in Figures 4 and 5) suggest only a single ripple. The wave is most visible at approximately right angles to the projected local vertical. The wave feature extends above the limb in projection, establishing that it is propagating in the corona (see also Figure 10). At later times a slower ejection moved more directly to the west, and appeared to have the more normal loop-like character of many flare ejecta observed by SXT. The path of the ejection was near the plane containing the local vertical (see Figure 5). The motion to the north that we identify as a wave has no obvious fixed footpoint locations, whereas the ejecta to the east are consistent with fixed footpoints and thus appear loop-like.

We have followed the X-ray wave in as much detail as possible in order to identify its region of origin (radiant point). In each of the images in which we can see the wave we traced the outermost wave feature. The arcs thus defined appear in Figures 8 and 9. As the wave moves out into the corona, the wavefronts tilt away from solar vertical, consistent with refraction in a coronal model with Alfvén speed increasing with height (Uchida, 1968).

To identify the radiant point and time of origin, we have made a reconstruction of ray trajectories following the Huygens principle (Wills-Davey and Thompson, 1999). We trace the rays by linearly fitting closest points on successive wavefronts which lead back to a common radiant point, and their intersections define the time
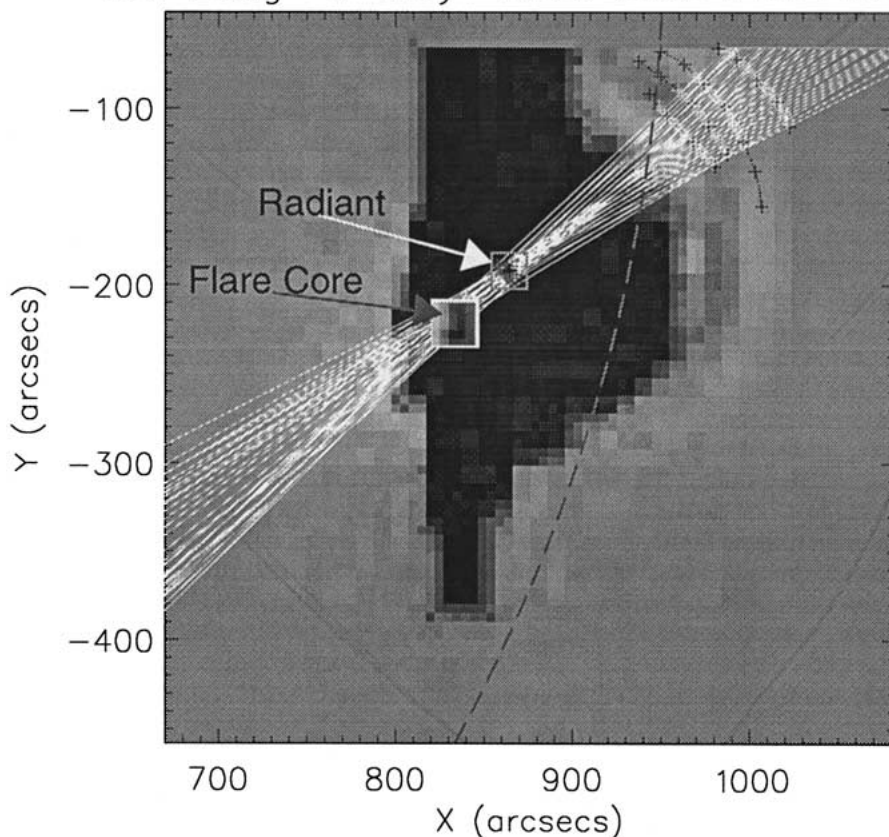
Figure 8. Wavefront analysis of the half-resolution AlMg data. *Black crosses* show the selected positions on the wavefronts for the several images, superposed on the difference image indicated. *White lines* show the projected rays at a set of points along the wavefronts. Their intersections define the radiant point and time of wave origin, and the mismatches result both from error and from wavefront tilt.

of origin. Figures 8 and 9 illustrate this analysis for the half-resolution and quarter-resolution data, respectively. The rays thus defined do extrapolate backwards to an apparent radiant location which lies at the expanding large loop feature (the boxed region shown in Figure 6) or between it and the flare core loops. The radiant locations are indicated by boxed regions in Figure 3. The mismatch of the rays, constructed from manual designation of the wave location on each image, serves as a guide to the errors of this technique. Note that we excluded the later wave fronts which exhibit the bending inferred to result from coronal refraction. The radiant times (listed in Table I) for the two image resolutions are 08:01:11 UT for quarter-resolution, and 08:02:06 UT for half resolution. These bracket the time of the inital hard X-ray burst seen in Figure 2. We believe that the position uncertainty
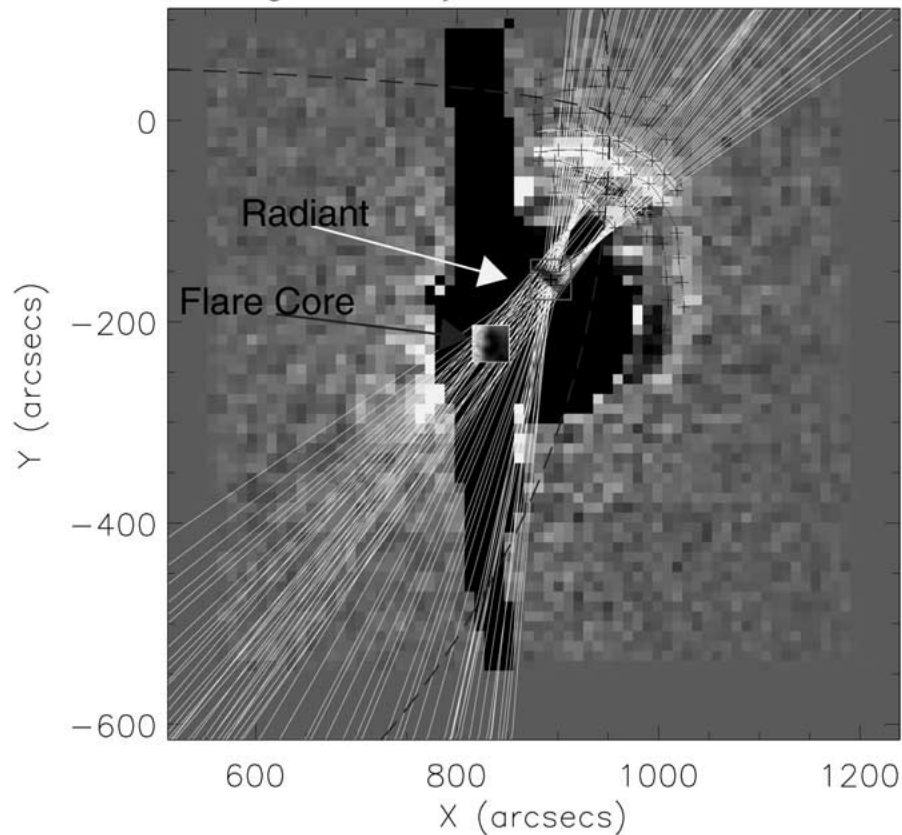
Figure 9. Same as Figure 8, but for the quarter-resolution AlMg data.

inferred from the scatter of the rays, though large, excludes the flare core loops as the direct source of the wave. In Section 4 we consider the timing in relationship to the growth of gas pressure in the flare core loops, coming to a similar conclusion.

3.3. SOHO EIT OBSERVATIONS

Biesecker *et al.* (2002) have recently studied 'EIT waves' systematically. They find a close association of the best-defined examples in their sample (category Q5, 'Clear propagation of front'), with flares and type II bursts, as well as CMEs. The 6 May event (Figure 10) matches the description given for events in this category. The closest EIT frame was obtained at 08:10.0 UT, about three minutes after the wave left the north edge of the SXT field of view. This is shown as a difference image relative to an image taken immediately prior to the flare at 07:58.3 UT. The image shows multiple ripple-like features in the direction of propagation of the sources seen by SXT, but extended over the location of the limb. The extension
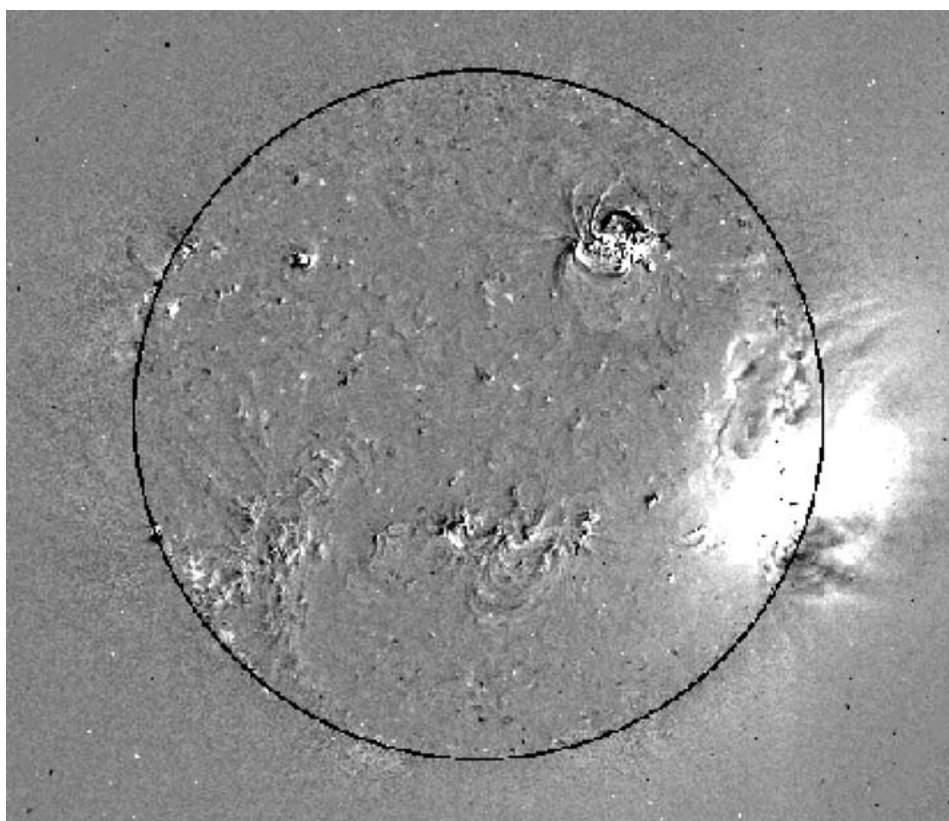
Figure 10. Difference image comparing two EIT exposures (08:10.0 UT minus 07:58.3 UT, thus showing the 195 Å corona about 8 min after the wave radiant time (see Table I)). We identify the ripple-like features crossing the limb, to the north of the flare site, with the emission front detected in the SXT images. The EIT wave features show the downward tilt also observed by SXT.

over the limb confirms the coronal nature of the disturbance in EUV as well as in soft X-rays. We note that the ripples do not appear concentric with respect to the flare core, confirming the anisotropy in velocity apparent from the SXT images (e.g., Figure 5) if we identify the SXT and EIT features with each other.

3.4. OTHER OBSERVATIONS

As listed in the *Solar-Geophysical Data*, this event had the full range of meter-wave properties expected for a large eruptive flare and CME. In Figure 11 we show the dynamic spectrum observed in the meter-decimeter range at Hiraiso (Kondo *et al.*, 1995). The type II emission has a ragged appearance, but with a bright onset near 300 MHz at about 08:05:30 UT. Making an identification of the observing frequency in the low-frequency branch of a type II burst at the local plasma frequency, we find that the brightening occurred at a density of $n_e \approx 10^9$ cm^{-3}. However a faint trace of slow-drift emission extends earlier to higher frequencies.
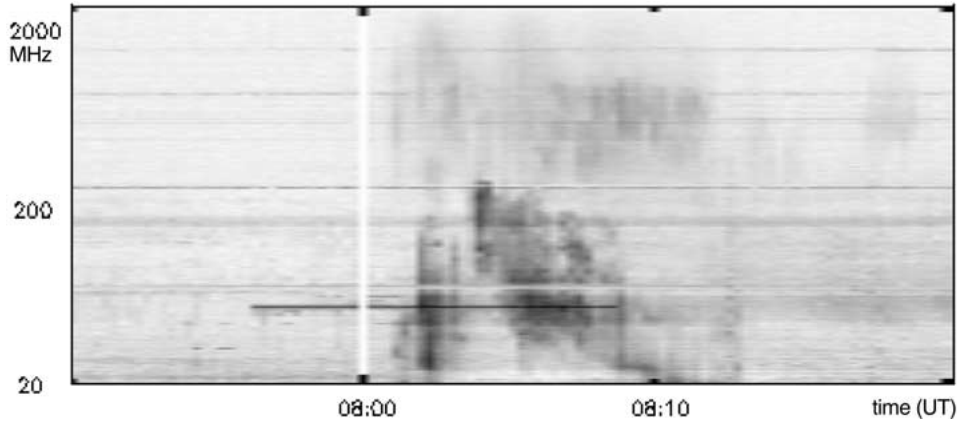
Figure 11. Meter-wave dynamic spectrum for the event of 6 May 1998 (long wavelengths at bottom), with a reversed intensity scale. Note the early decimetric extension of the slow-drift burst. We interpret the brightening at 200 MHz as the onset of the type II emission and call attention to earlier features at higher frequencies (courtesy CRL Hiraiso).

This decimeter source seems continuum-like rather than structured as noted for type II burst precursor bursts by Klassen *et al.* (1999). Similar decimetric continuum features have been reported by (Karlický, 1984; see also Hudson *et al.*, 2001 and Khan *et al.*, 2002). We have not done a detailed analysis of the radio signatures in this paper. The presence of the continuum feature suggests continuity of the excitation down close to the compact sources of the fast-drift bursts and hard X-rays. Emission at 2 GHz, starting at about 08:03:30 UT, implies a density above 10^{10} cm^{-3}, interpreting the emission as the harmonic of the local plasma frequency. This time is about 100 s after the peak of the initial hard X-ray burst.

4. Physical Parameters

4.1. FLARE CORE LOOPS

The SXT observations determine the emission measure EM ($n_e^2 V$) in each pixel, where n_e represents the electron number density and V the volume subtended by the pixel. This determination requires two sequential exposures with different filters (here we use Be and Al12), and assumes an isothermal medium (see Tsuneta *et al.*, 1991). We have estimated the density and pressure within the core flare loops by first determining the area of the loops at the 50% contour level in an image. We use this to estimate volume V (the 3/2 power), and hence the electron number density $n_e = \sqrt{EM/V}$ and the pressure $p_e = 1.9\, n_e kT$ (Priest, 1982, p. 82), at 08:07:58 UT, as listed in Table I. The time of increase of gas pressure in the loops makes an obvious point of comparison for theories of wave generation (e.g., Vršnak and Lulić, 2000a, b), so we have also listed a reference time for the increase
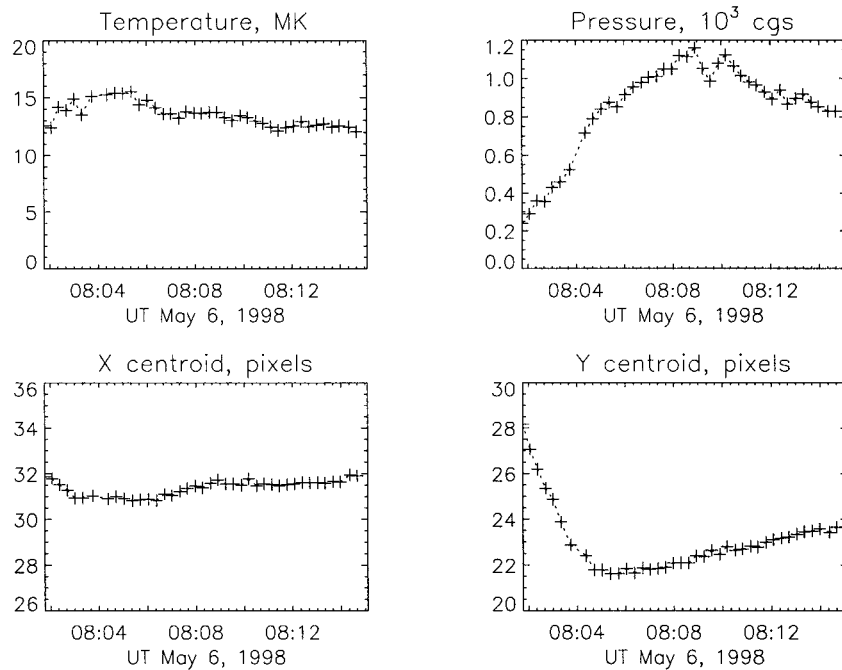
Figure 12. Variation of physical parameters of the flare core loops. Temperature and pressure are derived from the SXT filter ratio Be/Al12, assuming isothermality, by taking the volume as the 3/2 power of the projected area. For the centroid motions (X to the west, Y to the north), one SXT pixel corresponds to 1.80 Mm.

of electron pressure in Table I. The other loop quantitities in Table I also refer to this particular time. Figure 12 gives the time variation of estimated pressure in the core loops along with other physical parameters.

The variation of apparent electron pressure p_e with time shows a gradual increase, with a broad maximum at about 08:07:20 UT. We would like to assess this pressure increase as a 'pressure pulse' capable of launching the wave. To place a time reference on the occurrence of the pulse, we could adopt the half-pressure time of approximately 08:04 UT; a polynomial fit to the data (not shown here) suggests a broad maximum in the time derivative at about the same time.

In contrast the image morphology changes rapidly near the beginning of the event. Movies of the images and the plots of X and Y centroid locations given in Figure 12 reveal only slight motions EW, but a large motion NS. This motion happens within the nearly fixed outline of the loop structure itself, which at the resolution of the observations does not show an increase in size that could be attributed to the pressure growth.

The *Yohkoh* soft X-ray data have sufficient resolution often to detect impulsive brightenings at the loop footpoints (McTiernan *et al.*, 1993; Hudson *et al.*, 1994). We find a suggestion of similar behavior in this flare, but the footpoints do not
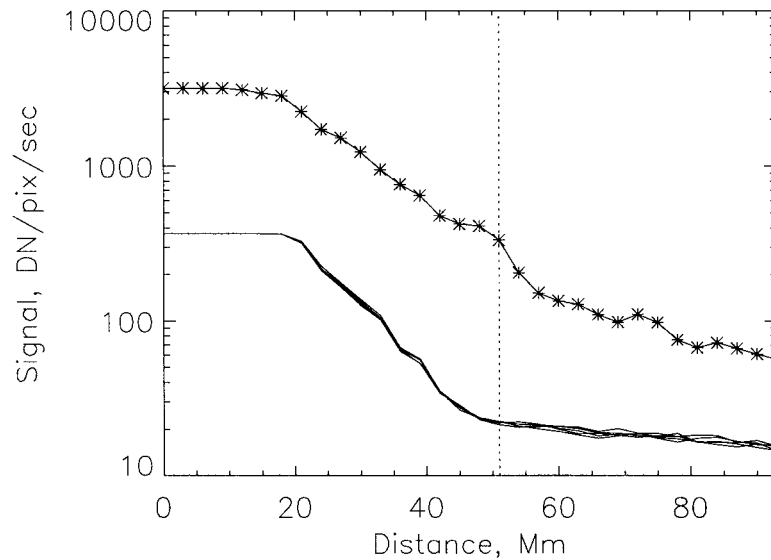
Figure 13. Brightness variation along a line tilted 30° W, passing through the flare core, to show the flare image brightness relative to the preflare levels. The *upper trace* shows the trace from a single image (08:04:14 UT). The *lower traces* show several pre-flare exposures, establishing the lack of variation. The *dotted vertical line* shows the location of the emission-measure estimates described in the text, with the wave enhancements visible as inflection. Most of the signal in the flare image, even at great distances from the flare core, results from scattered light. The flat levels interior to 20 Mm result from image saturation.

appear as bright discrete sources. The northern footpoint region of the flare core loops brightens suddenly between 08:03 and 08:04 UT, as noted in Table I.

4.2. THE WAVE

We use the observed coronal signal to estimate the temperature amplitude and Mach number of the wave, as summarized in Table II. The best data for this purpose are the quarter-resolution images, which we can compare directly with preflare images at the same resolution and with the same filter. We select a point along a line inclined 30° west of north, at a distance of 120 Mm from the flare core, at which to compare the preflare and flare signal levels. The intensity jump corresponds to an intensity increase of about a factor of 6 relative to pre-flare levels. The emission-front signal rides on top of an enhanced background level due to scattering of flare X-rays from the SXT mirror. Assuming the ambient coronal temperature to be 2.5 MK we find that the emission measure at the peak brightness would correspond to an increase in emission measure $n_e^2 \ell$ from 9.0×10^{25} to 5.4×10^{26} cm^{-5}. For an assumed line-of-sight path length of 50 Mm and unit filling factor, the background coronal intensity corresponds to a density of $n_e = 2 \times 10^8$ cm^{-3}.

TABLE II

Estimates of Mach number.

$T_{ambient}$	T_{wave}	Jump	Mach number
1.58 MK	1.8 MK	1.14	1.09
1.99	2.5	1.25	1.16
2.51	3.4	1.38	1.26
3.16	4.7	1.48	1.33
3.98	6.6	1.65	1.44

5. Interpretation

These observations give us a first detailed view, at high resolution, of flare disturbances that lead to a coronal shock wave. We would like to interpret these observations with respect to three major questions: (i) is the wave-like motion we see actually the wavefront that later shocks to become the type II burst, or is it ordinary flare loop ejecta; (ii) if a wave is it a blast wave, or is it driven by ejecta; and (iii) is the cause of the wave a 'pressure pulse' (restrained motion; for a possible SXT example, see Green *et al.*, 2002), or is it the initial motion of an ejection (see Nitta and Akiyama, 1999, for examples). We discuss each of these questions in the following sections, after first commenting on the observed wave intensity.

5.1. INTENSITY

The 6 May event was surprisingly intense, roughly a factor of two brighter than even the high background level resulting from scattered flare X-rays. We have estimated it to be roughly an order of magnitude more intense than the preflare quiet corona outside the region of flare brightening (see Figure 13). Such a large intensity enhancement might seem to be inconsistent with Uchida's description of such a wave as a 'weak shock'. However, our analysis of wave detectability by SXT (see Appendix A) would allow amplifications by such a factor for $0.3 < \Delta T/T < 1.5$, depending upon ambient coronal temperatures within a reasonable range. This estimate is based on assuming an adiabatic coupling between the wave density and temperature (e.g., Priest, 1982). Within this approximation, we find the electron temperature in the wave to lie in the range 2–4 MK, and for the Mach number of the shock to lie in the range 1.1–1.3 at the reference point of observation (Table II). These estimates depend upon the assumed ambient coronal temperature (first column of Table II). Such values of the Mach number seem reasonable based upon studies of type II bursts (e.g., Nelson and Melrose, 1985). The temperatures and Mach numbers have large errors but are essentially lower limits because of our lack of detailed geometrical knowledge (the filling factor) to relate the X-ray emis-

sivity to the observed flux. Within the broad limits of our knowledge of the wave geometry and the plasma physics, we believe that the observation is consistent with interpretation of the X-ray emission front as the signature of a coronal shock wave at low Mach number.

A similar analysis of the wave intensity could be done for the EUV observations. It would be complicated by the narrow-band temperature response of the EIT and TRACE passbands; in principle a compressive heating could result in either a brightening or a dimming depending upon the ambient temperature.

5.2. WAVES OR LOOPS?

In the absence of other information, it is difficult to distinguish a wave from an expanding loop in the SXT images. This is especially so since the wave studied here is only a sector, rather than a full ring, and since temperature variations often make loop footpoints difficult to detect. However, the morphology here strongly suggests a wave. Its initial development is concentric on a radiant point or compact region, and it shows no fixed footpoints. The most obvious motion is roughly perpendicular to the direction of the subsequent loop-like flare ejecta. The apparent speed of the wave exceeds that of the ejecta in this event, although flare ejecta in other events may have comparable speeds. In spite of these points of consistency with a wave interpretation, it would be possible for this just to represent an unusual set of loop ejecta, if we only considered the soft X-ray data; in other words, we do not feel that the X-ray data alone are unambiguous on this point. However, the EIT data show ripples in the direction of propagation of the X-ray wave, and in between the SXT and EIT observing times, the meter-wave data show the onset of a type II burst at a frequency consistent with an appropriate coronal density. The X-ray wave fronts tilt in the manner expected for fast-mode MHD wave refraction. Finally, the decimeter spectrum also shows a drifting feature prior to the type II onset, at an inferred density consistent with that of the corona at the wave location. Based on all this direct and indirect evidence, we believe that the X-ray data show the direct effects of wave propagation.

5.3. LAUNCHED BY A PRESSURE PULSE OR BY AN EJECTION?

It is possible to create a coronal wave via a pressure pulse (e.g., Vršnak and Lulić, 2000a, b), and near the origin of the 6 May wave we indeed see a rapidly-increasing gas pressure in the flare core loops. We have given some parameters of this pressure increase in Table I. The timing of the pressure increase does not favor a wave source at the core loop, an argument consistent with the kinematics discussed in Section 3.2. The radiant point is significantly displaced from the core loop region, and the radiant time significantly earlier than the observed pressure rise.

The parameter plots shown in Figure 12 show the centroid positions of the flare core loops as a function of time. A pressure pulse would be effective in launching a wave if it displaced the magnetic structure above it. The EW centroid position

(roughly interpretable as loop height) shows no jump outward corresponding to the pressure increase, suggesting low plasma β and no wave generation. The NS centroid, on the other hand, moves rapidly (~ 100 km s^{-1} projected) to the south during the formation time of the wave. The images suggest that this results from motion along the field lines rather than perpendicular, i.e., flows consistent with chromospheric evaporation. This could be interpreted as the source of the wave motion, as proposed by Karlický (1998), except that the apparent velocity is low and is in a different direction. We also detect an impulsive soft X-ray brightening close in time to the radiant time of the wave, and directly beneath the rapidly expanding bubble we associate with the wave origin. These features occur almost simultaneously, within errors on the order of 10 s, so they could well be related to the launching of the wave. Based on this evidence, we believe that a pressure pulse in the later flare core loops themselves cannot explain the observations.

5.4. BLAST WAVE OR DRIVEN WAVE?

The X-ray wave moves rapidly away from the apparent exciter, identified with the radiant point inferred from Figures 9 and 10. The flare ejecta move in a substantially different direction, as displayed in Figures 4 and 5, and at a lower speed (approximately 300 km s^{-1}; we have not done a full analysis of the flare ejecta for this paper). In the case of a driven wave, we would expect a closer match in speed, direction, position and time between the exciter and the wave. They appear to be separate phenomena, even though they both arise in the flare. Based on this mismatch, we do not see any evidence that the wave is driven by the ejecta that we see to the west of the flare, and conclude that it is a blast wave. At the radiant point we do see outward material motions but cannot follow them as an ejection into the region traversed by the wave.

5.5. SHOCK WAVE OR NOT?

Type II bursts typically display a sudden increase in brightness, associated theoretically with the moment of conversion of the wave disturbance to a shock. The moment of turn-on is somewhat ambiguous, but characteristic precursor features may also be a guide (Klassen *et al.*, 1999). At this point the Mach number would be low, but as the blast wave propagates outward it may increase. Our observations show wave motion *prior* to the apparent turn-on of the type II emission (Figure 11, where we suggest the sudden brightening at $200-300$ MHz to be the shock ignition time). Accordingly, before this time the Mach number was near unity. We believe that this is a guide to the errors inherent in our analysis (Table II), based on the assumption of a quasi-perpendicular MHD fast-mode shock. It also establishes that a wave of this type is a weak shock, rather than a strong shock (see Wang, 2000, for a different conclusion based on EIT waves). Narukage *et al.* (2002) report another SXT wave observation, this one in coincidence with a Moreton wave, with similar properties.

6. Conclusions

Based upon the appearance of the SXT observations, our analysis of the required Mach number for the emissivity jump observed, and upon the continuity observed with the type II burst and EIT observations, we conclude that the SXT data show soft X-ray emission from the wave itself. The X-ray phenomenon can be explained by a flare-induced blast wave, and give a glimpse of material motion associated with its launching. The perspective on the limb enables us to note that it refracts towards the chromosphere, implying an Alfvén speed increasing with height. The wave may be identified with the source of the metric type II emission and possibly with an earlier drifting decimetric feature. The direct detection of the wave in the *Yohkoh* SXT soft X-ray images gives estimates of the Mach number, which fall in the expected range.

Wavefront analysis of the soft X-ray observations allow us to establish a time and position for the radiant of the wave. This analysis confirms the close association of the wave excitation with the beginning of the impulsive phase of the flare, and suggest that the wave may come from plasma motions that begin at a relatively small distance (within ~ 20 Mm, ~ 0.03 $R_{\odot}$) from the flare core. The radiant point is however significantly displaced from the flare core. In the vicinity of the radiant point, we observe a faint slowly-moving feature, but the most striking association is with the sudden outward motion of a previously-existing large loop structure. These phenomena are adjacent to but not obviously connected with the bright core loops of the flare itself. The wave does not appear to arise in a pressure pulse occurring in the core loops of the flare, either on kinematic evidence or from an analysis of the physical parameters of these loops. We speculate that the magnetic restructuring that these motions reveal may release the energy of the early loop brightening. The X-ray images show only outward motions in this phase of the flare, tending to rule out an implosion (Hudson, 2000) as the source of the wave disturbance.

We have reviewed the factors that make X-ray wave detection difficult. Scattered light, photon statistics and CCD dynamic range play important roles, and the common occurrence of ejecta – with similar speeds – make it difficult to distinguish the wave motion itself. The main obstacle to soft X-ray wave detection seems to be the presence of scattered light in the grazing-incidence optics of SXT. We find that the monotonically increasing SXT response as a function of temperature actually amplifies the effect of a wave disturbance. We, therefore, expect further X-ray wave detections (e.g., Khan and Aurass, 2002). These should help us to learn empirically about the exciting disturbances as well as about coronal properties from their propagation characteristics.

Finally, the 6 May event gives us further confidence about the identification of some EIT wave features with the fast-mode shock theory of Uchida (1968). At the time of writing, there have been several reported matches (in time and location) among EIT waves, Moreton waves, type II bursts, and now waves seen directly in

soft X-rays. Based on these examples, it seems clear that EIT waves have multiple physical explanations, including both the classical fast-mode waves propagating in an undisturbed corona, and also large-scale structural changes in the medium itself (Delannée and Aulanier, 1999).

Appendix A. Factors Relevant to Wave Detection

In this section we discuss the problem posed by the fact that *Yohkoh* SXT has not observed many global wave events. Several factors contribute to this problem, which is quite striking considering the relative ease with which the SOHO EIT instrument makes large-scale wave observations. The EIT (Delaboudinière *et al.*, 1995) is a normal-incidence EUV telescope, and most of the wave observations take place in the 195 Å passband centering on an Fe XII line. The factors that distinguish these two sets of observations include the plasma physics of the radiative process, the behavior of the telescope optics, including wavelength selection, and the method of sampling. In the following we will not discuss EIT in detail except where the comparison is relevant to the SXT observations.

A.1. PLASMA PHYSICS AND SPECTRAL RESPONSE

The SXT images show soft X-ray emission from the diffuse ambient corona as well as in the hot, dense active-region loops. When a compression wave passes a point in this medium, it will produce a local increase of temperature and density. Both factors contribute directly and indirectly (via the resulting adjustment of the ionization states and particle distribution functions) to a change in the X-ray emissivity, including its spectral distribution. We discuss these matters in Section B.

A.2. OPTICS AND SCATTERED LIGHT

The SXT observations, especially near flares, suffer from strong scattering effects (see Tsuneta *et al.*, 1991). This is a result of the short wavelengths observed, which has important consequences. First, the scattering increases with the ratio of mirror

roughness to observing wavelength (in a grazing-incidence geometry, foreshortening can make this problem much worse in the mirror radial direction). This is a function of off-axis angle; the angle of incidence for SXT varies around 1.07°. Second, the solar X-ray spectrum generally decreases rapidly with increasing photon energy, especially at high temperatures where continuum begins to dominate. Thus the contrast of hot, compact flare features becomes extremely large relative to the quiet corona, exacerbating the scattering problem. The representation of SXT images with full dynamic range normally requires a logarithmic scaling covering six decades of surface brightness (e.g., Acton *et al.*, 1992). Normal-incidence telescopes at longer wavelengths (SOHO EIT or TRACE) do not suffer so severely from these problems.

A.3. PHOTON STATISTICS

Each X-ray photon makes many hole-electron pairs upon absorption in the silicon of the CCD detector. By contrast, an EUV instrument operates at a longer wavelength, for example 195 Å, so there are fewer pairs per photon. This increases the photon detection rate by an order of magnitude.

A.4. CCD DYNAMIC RANGE

For typical ambient temperatures and an SXT 'thin' X-ray analysis filter (either Al.1 or AlMg), one photon corresponds to about 2.4 DN (data number), as compared with a saturation level of 4096 DN (depending on the on-chip summing mode). This information is available via the routine SXT_FLUX in SolarSoft (Freeland and Handy, 1999). Thus the image dynamic range, estimated (for example) between 100 photons per pixel (10% statistics) and 4096 DN (full well), must be less than two decades for any single exposure. SXT can make multiple exposures with widely different exposure times in order to compensate for this problem, but typical images during flares have automatic exposure control, to avoid saturation or damage, and are therefore short ones. In practice this makes it difficult to see the ambient corona in flare-mode observations.

A.5. FLARE MODE

In *Yohkoh's* normal operations, a special flare mode starts when the soft X-ray flux passes a given threshold, roughly equivalent to the C2 level in GOES photometry. Data prior to this time may have low resolution, may be overwritten by the higher-priority flare data, or may refer to a non-flaring active region. During flare mode SXT takes only partial-frame images. Thus normally we can only study global effects well during flares at the C2 level or below; the full-frame images outside flare mode normally have a full cycle time of 8 min, resulting in a major sampling penalty.

A.6. THE SAMPLING 'VELOCITY FILTER'

The *Yohkoh* Soft X-ray Telescope (SXT) normally observes flares in a restricted field of view. The image scale and sampling cadence thus impose a velocity filter on the detection of a large-scale wave. At 1000 km s^{-1}, the standard sampling (a square field of view 4.60×10^{10} cm on a side, typically observed at intervals of ~ 20 s) would provide at most about ten consecutive images of a disturbance starting at its center. Given typical image saturation near the core of the flare, a wave at twice the speed would be almost non-measurable.

A.7. CONFUSION WITH MASS MOTIONS

Flares, especially major ones, often are *ejective*, with motions related to CMEs taking place. We know that many of these motions are not wave-like and involve the physical displacement of magnetic loops, and probably their re-formation via reconnection. Such physical motions have speeds not so different from the speed of an MHD blast wave with low Mach number.

To summarize, several instrumental effects control the detectability of a wave by SXT. Any given SXT image has a limited dynamic range imposed by the relatively large energy deposition of a single X-ray photon in the CCD, and by the CCD's full-well limit. A photon count of ten per pixel, plus dark current, amounts to roughly one percent of an optimum exposure level. The images studied here have fixed exposure levels in order to show faint features, and because the flare magnitude cannot be predicted, this exposure time (normally 38 ms) may not be optimal. For a large flare, all SXT images have scattered-light contributions from the flare core, at a level depending upon the flare brightness and temperature distribution. Finally, flare-mode timing depends upon the total soft X-ray flux, so that SXT seldom observes the earliest phase of a flare, unless a coincidental earlier flare has left the instrument in flare mode already. These factors conspire to make it more difficult for SXT to observe large-scale waves, as compared with EIT.

Appendix B. SXT Response to a Wave

How would a large-scale coronal wave be detected in an SXT image? Tsuneta *et al.* (1991) present response functions for the different SXT X-ray analysis filters. These typically show a monotonically rising response as a function of temperature, with the response leveling off or falling slowly above several MK in the range of ordinary coronal temperatures. A compression wave would increase the electron temperature T_e simultaneously with the density n_e, and would accordingly result in an increased soft X-ray brightness. A rarefaction would have the opposite effect. We can write the SXT response function as

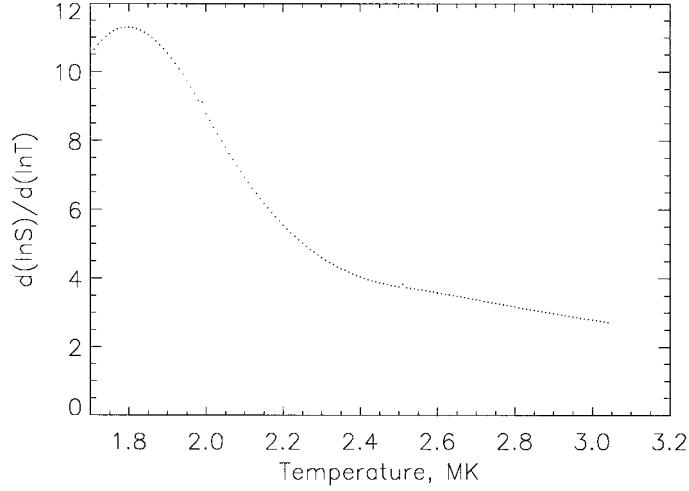$$R_i(n, T_e) = \text{const.} \times n_e^2 \times S_i(T_e), \qquad (1)$$

Figure 14. SXT response (AlMg filter) to a temperature variation, expressed as a log derivative assuming adiabatic conditions with polytropic index 5/3.

where the index i represents the particular X-ray filter used to select the spectral passband, and the functions $S_i(T_e)$ contain all of the necessary information on spectral response, including the atomic physics and ionization equilibrium calculations, as assumed in the standard *Yohkoh* software. For a given ambient coronal temperature and for the assumption of an adiabatic variation (valid only for small Mach number), we can summarize the differential version of this relationship as

$$\frac{\partial(\ln(R_i))}{\partial(\ln(T_e))} = \Delta_i(T_e) = 3 + \frac{d(\ln(S_i))}{d(\ln(T_e))}, \qquad (2)$$

with the logarithmic derivative $\Delta_i(T_e)$ varying with ambient temperature T_e for the ith SXT X-ray analysis filter. Figure 14 shows the temperature dependence of Δ_3, the response of the AlMg X-ray analysis filter used in the SXT observations described in this paper. Equation (2) assumes a polytropic index 5/3. For ambient coronal temperatures, the logarithmic derivative remains positive (and large); accordingly, SXT should show a maximum at the compression peak of the wave. Because the corona is optically thin in soft X-rays, the signal would represent an integration through an unknown geometrical structure. We assume that the wave propagation will differ from point to point in the highly inhomogeneous corona. Ideally we would expect a sharp peak if the line-of-sight were tangent to a smooth global wavefront. Finally, we note that the rapid passage of a fast-mode shock in the low-density corona may not allow time for a high-Z element, such as those that contribute strongly to the SXT response via emission lines, to come into ionization equilibrium. Accordingly there is a presently unknown uncertainty in the values of $\Delta_i(T_e)$, which could however be modeled in detail.

To estimate the signal increase directly (rather than differentially), we can write
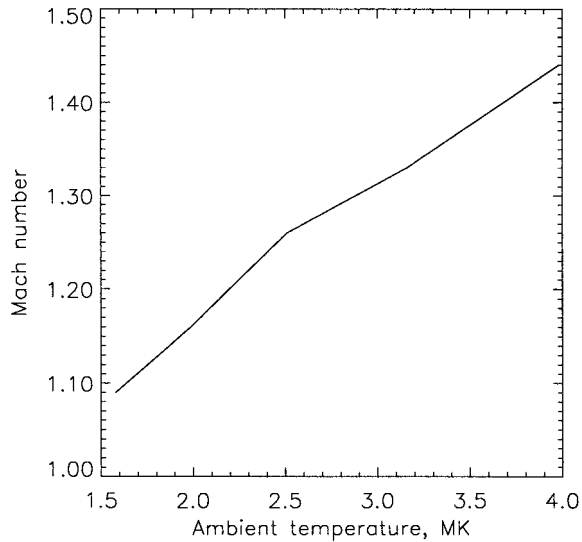
Figure 15. Mach number of a wave resulting in an SXT intensity increase (AlMg filter) of a factor of 6, as a function of ambient temperature.

$$\frac{S_1}{S_2} = \frac{T_{e1}^3 S_i(T_{e1})}{T_{e2}^3 S_i(T_{e2})},$$
(3)

where the T_e^3 factor comes from the density variation (downstream and upstream quantities denoted by 1 and 2, respectively) under the adiabatic approximation. Figure 15 shows the estimated Mach number for a wave required to make a six-fold signal increase in the AlMg filter, as observed in the event discussed in this paper. Although these must be interpreted as lower limits (see the Discussion in the main text), it appears that a Mach number of order $1.1–1.2$ would be consistent with the ambient coronal temperature.

For EIT the observing situation is similar, but the response of the 195 Å pass-band commonly used for wave observations has a sharply peaked response as a function of temperature around Fe XII emission lines. The wave-induced signal would, therefore, depend upon the excitation temperature prior to the wave; the peak of a compressive wave could be either relatively bright or relatively dark in a given pixel, depending on the ionization distribution.

References

Acton, L. W., Tsuneta, S., Ogawara, Y., Bentley, R., Bruner, M., Canfield, R., Culhane, L., Doschek, G., Hiei, E., and Hirayama, T.: 1992, *Science* **258**, 618.

Biesecker, D. A., Myers, D. C., Thompson, B. J., Hammer, D. M., and Vourlidas, A.: 2002, *Astrophys. J.* **569**, 1009.

Cliver, E. W., Webb, D. F., and Howard, R. A.: 1999, *Solar Phys.* **187**, 89.

Delaboudinière, J.-P. *et al.*: 1995, *Solar Phys.* **162**, 291.

Delannée, C. and Aulanier, G.: 1999, *Solar Phys.* **190**, 107.

Freeland, S. L. and Handy, B. N.: 1999, *Solar Phys.* **182**, 497.

Gopalswamy, N., Kundu, M. R., Manoharan, P. K., Raoult, A., Nitta, N., and Zarka, P.: 1997, *Astrophys. J.* **486**, 1036.

Green, L. M., Matthews, S. A., van Driel-Gesztelyi, L., Harra, L. K., and Culhane, J. L.: 2002, *Solar Phys.* **205**, 325.

Harvey, K. L., Martin, S. F., and Riddle, A. C.: 1974, *Solar Phys.* **36**, 151.

Hudson, H. S.: 2000, *Astrophys. J.* **531**, L75.

Hudson, H. S. and Karlický, M.: 2000, in R. Ramaty and N. Mandzhavidze (eds.), *High Energy Solar Physics - Anticipating HESSI, ASP Conf. Ser.* **206**, 268.

Hudson, H. S. and Webb, D. A.: 1997, in N. Crooker, J. Joselyn, and J. Feynman (eds.), *Coronal Mass Ejections: Causes and Consequences, Geophysical Monographs* **99**, 27.

Hudson, H. S., Acton, L. W., and Freeland, S. L.: 1996, *Astrophys. J.* **470**, 629.

Hudson, H. S., Strong, K. T., Dennis, B. R., Zarro, D., Inda, M., Kosugi, T., and Sakao, T.: 1994, *Astrophys. J.* **422**, L25.

Hudson, H. S., Kosugi, T., Nitta, N. V., and Shimojo, M.: 2001, *Astrophys. J.* **561**, L211.

Kai, K.: 1969, *Solar Phys.* **10**, 460.

Karlický, M.: 1984, *Solar Phys.* **92**, 329.

Karlický, M.: 1998, *Astron. Astrophys.* **338**, 1084.

Kerdraon, A. and Delouis, J.-M.: 1997, in G. Trottet (ed.), *Coronal Physics from Radio and Space Observations, Lecture Notes in Physics* **483**, 192.

Khan, J. I. and Aurass, H.: 2002, *Astron. Astrophys.* **383**, 1018.

Khan, J. I. and Hudson, H. S.: 2000, *Geophys. Res. Lett.* **27**, 1083.

Khan, J. I., Vilmer, N., Saint-Hilaire, P., and Benz, A. O.: 2002, *Astron. Astrophys.* **388**, 363.

Klassen, A., Aurass, H., Klein, K.-L., Hofmann, A., and Mann, G.: 1999, *Astron. Astrophys.* **343**, 287.

Klein, K.-L., Khan, J. I., Vilmer, N., Delouis, J.-M., and Aurass, H.: 1999, *Astron. Astrophys.* **346**, L53.

Klimchuk, J. A., Acton, L. W., Harvey, K. L., Hudson, H. S., Kluge, K. L., Sime, D. G., Strong, K. T., and Watanabe, Ta.: 1994, in Y. Uchida, T. Watanabe, K. Shibata, and H. S. Hudson (eds.), *X-ray Solar Physics from Yohkoh*, Universal Academy Press, Tokyo, p. 181.

Kondo, T., Isobe, T., Igi, S., Watari, S., and Tokumaru, M.: 1995, *J. Commun. Res. Lab.* **42**, 111.

McTiernan, J., Kane, S. R., Loran, J. M., Lemen, J. R., Acton, L. W., Hara, H., Tsuneta, S., and Kosugi, T.: 1993, *Astrophys. J.* **416**, L91.

Moore, R. L. and LaBonte, B. J.: 1985, *Proc. Symposium on Solar and Interplanetary Dynamics*, D. Reidel Publ. Co., Dordrecht, Holland, pp. 207–210.

Moreton, G. E.: 1960, *Astron. J.* **65**, 494.

Moreton, G. E.: 1961, *Sky Telescope* **21**, 145.

Moreton, G. E. and Ramsey, H.E.: 1960, *Publ. Astron. Soc. Pacific* **72**, 357.

Moses, D. and 35 co-authors: 1997, *Solar Phys.* **175**, 571.

Narukage, N., Hudson, H. S., Morimoto, T., Akiyama, S., Kitai, R., Kurokawa, H., and Shibata, K.: 2002, *Astrophys. J.* **572**, L109.

Nelson, G. J. and Melrose, D. B.: 1985, in D. J. McLean and N. R. Labrum (eds.), *Solar Radiophysics*, Cambridge University Press, Cambridge, p. 333.

Nitta, N. and Akiyama, S.: 1999, *Astrophys. J.* **525**, L57.

Pohjolainen, S., Maia, D., Pick, M., Vilmer, N., Khan, J. I., Otruba, W., Warmuth, A., Benz, A., Alissandrakis, C., and Thompson, B. J.: 2001, *Astrophys. J.* **556**, 421.

Priest, E.: 1982, *Solar Magnetohydrodynamics*, Cambridge University Press, Cambridge.

Ramsey, H. E. and Smith, S. F.: 1966, *Astron. J.* **71**, 197.

Rust, D. M. and Hildner, E.: 1978, *Solar Phys.* **48**, 381.

Sheeley, N. R. Jr. and 18 co-authors: 1997, *Astrophys. J.* **484**, 472.

Thompson, B. J., Plunkett, S. P., Gurman, J. B., Newmark, J. S., St. Cyr, O. C., and Michels, D. J.: 1998, *Geophys. Res. Lett.* **25**, 2465.

Thompson, B. J., Gurman, J. B., Neupert, W. M., Newmark, J. S., Delaboudinière, J.-P., St. Cyr, O. C., Stezelberger, S., Dere, K. P., Howard, R. A., and Michels, D. J.: 1999, *Astrophys. J.* **517**, L151.

Thompson, B. J., Reynolds, B., Aurass, H., Gopalswamy, N., Gurman, J. B., Hudson, H. S., Martin, S. F., and St. Cyr, O. C.: 2000a, *Solar Phys.* **193**, 161.

Thompson, B. J., Cliver, E. W., Nitta, N., Delannée, C., and Delaboudinnière, J.-P.: 2000b, *Geophys. Res. Lett.* **27**, 1431.

Tsuneta, S. and 13 co-authors: 1991, *Solar Phys.* **136**, 37.

Uchida, Y.: 1968, *Solar Phys.* **4**, 30.

Uchida, Y.: 1974, *Solar Phys.* **39**, 431.

Vršnak, B. and Lulić, S.: 2000a, *Solar Phys.* **196**, 157.

Vršnak, B. and Lulić, S.: 2000b, *Solar Phys.* **196**, 181.

Wang, T., Yan, Y., Wang, J., Kurokawa, H., and Shibata, K.: 2002, *Astrophys. J.* **572**, 580.

Wang, Y.-M.: 2000, *Astrophys. J.* **543**, L89.

Wild, J. P., Smerd, J. F., and Weiss, A. A.: 1963, *Ann. Revs. Astron. Astrophys.* **1**, 291.

Wills-Davey, M. J. and Thompson, B. J.: 1999, *Solar Phys.* **190**, 467.